



University of Guilan

journal homepage: <https://cse.guilan.ac.ir/>

The Effect of Double Moving Walls on the Heat Transfer Enhancement of the Flow Around a Single Cylinder: Numerical Investigation

Amir Kiyumarsioskouei^{a,*}, Narjes Ghasemnezhad^a, Nabi Mehri Khansari^a^a Faculty of Mechanical Engineering, Sahand University of Technology, Tabriz, Iran

ARTICLE INFO

Article history:

Received 12 May 2024

Received in revised form 15 June 2024

Accepted 24 June 2024

Available online 24 June 2024

Keywords:

flow fluctuations

vortex shedding

flow around a circular cylinder

velocity and heat boundary layer

ABSTRACT

This research investigates the influence of wall proximity on convective heat transfer and fluid flow characteristics in a two-dimensional laminar regime around a circular cylinder. Six unique configurations, comprising various combinations of nearby and distant walls, are examined through numerical simulation. Assumptions related to incompressibility, viscosity, transiency, and Newtonian behavior inform the underlying fluid mechanics model. Governing equations encompass conservation principles for mass, momentum, and thermal energy. Applying the finite volume approach within a commercial computational framework facilitates numerical solutions for each test condition. A notable outcome indicates how the spacing between the cylinder and adjacent surfaces affects the drag force coefficient, revealing marked differences based on cylinder placement – either nestled between two stationary planes or situated near a singular bounding wall. Increasing interlayer frictional forces instigate reductions in fluid velocity, leading to diminished drag coefficients at higher Reynolds numbers. Moreover, implementing comparative analyses elucidates the substantial enhancements in the Strouhal number (by 44%), the Nusselt number (by 14%), the drag coefficient (by 108%), and the lift coefficient (by 112%) experienced by a confined cylinder suspended between two quiescent plane surfaces, contrasted against an isolated cylinder devoid of neighboring constraints. Collectively, these observations accentuate the significance of the particular arrangement wherein the cylinder exists equidistant between two motionless walls.

1. Introduction

For several decades, the examination of fluid flow and heat transfer phenomena surrounding cylindrical geometries has remained a focal point of exploration within the realm of mechanical engineering. Scholars have consistently sought to dissect and comprehend the intricacies of convective heat transfer processes encircling cylinders to effectively elucidate their overall thermal performance. Initial investigations predominantly centered around discerning the nuances

* Corresponding author.

E-mail addresses: kiumarsi@sut.ac.ir (A. Kiyumarsioskouei)

of heat transmission across cylinders submerged in diverse flow regimes, namely laminar and turbulent flows. Researchers studied the effects of cylinder diameter, flow velocity, and fluid properties on heat transfer. In this context, various methods are used to study flow and heat transfer around circular cylinders. Computational fluid dynamics (CFD) is an effective method for solving various engineering problems. In recent decades, many articles have studied the flow field and heat transfer around cylinders using CFD simulations [1]. The correlation between experimental results and numerical simulations for studying flow and heat transfer around cylinders is a significant milestone in this research field [2]. Vortices are formed as a result of physical disturbances imposed for a short period and after a transitory period, it becomes periodic [3]. These vortex structures behind circular cylinders or airfoils have a significant impact on lift and drag coefficients, heat transfer, vibrations and noise issues [4-6]. Many studies are being conducted on suppressing the shedding of vortices behind circular cylinders. Lie et al. [7] positioned the circular cylinder asymmetrically between two side walls to suppress vortex shedding in a numerical study. According to [8], a wide variety of aerodynamic and hydrodynamic means for suppressing vortex shedding is classified into three categories in accordance with the phenomenological mechanism of vortex shedding. The three categories are as follows: 1) Surface protrusions, which affect separation lines and/or separated shear layers, e.g. Helical strakes, wires, fins, studs or spheres, etc. 2) Shrouds, which affect the entrainment layers, e.g. perforated, gauze, axial-rod, axial-slat, etc. 3) Near wake stabilizers, which prevent interaction of entrainment layers, e.g. splitter plates, guiding vanes, base-bleed, slits cut across the cylinder, etc. because in the core of wake region, the fluctuations of velocity can reach 80 % of the free-stream velocity [9]. As an example, in the research done by Bouakkaz [10], the heat transfer and air flow around an unconfined heated rotating circular cylinder have been investigated numerically for varying rotation and suppression of vortex shedding occurs as the rotation rate increases. In research [11], Numerical simulations of incompressible laminar flow past a circular cylinder using wavy wall confinement are performed in order to study drag reduction and vortex shedding, The minimum drag coefficient and complete vortex shedding suppression (zero lift coefficient). The lift coefficient remains zero at all Reynolds numbers and blockage ratios which indicates complete suppression of vortex shedding. In a study by Tenda et al. [12] The vortex street behind a circular cylinder was investigated experimentally in a water tank. They found that: (1) walls increase the stability of the foundation; (2) Two parallel walls have a compression effect on the vortex street. (3) A single row vortex street is formed near a plane wall, which is consistent with [13]. Also, in a study conducted for a circular cylinder in subcritical flow conditions, it was shown that the friction coefficient and Nusselt number are functions of Reynolds number and surface roughness. Triangular roughness elements on the cylinder body stabilize boundary conditions, and the maximum drag reduction is observed for average roughness compared to a smooth surface [14]. Computations were also performed to determine the optimal conditions for the suppression of vortex shedding from circular cylinders at high and low Reynolds numbers by means of splitter plates. In many studies on this mechanism for two-dimensional flows with low Reynolds numbers and limited to a single ratio of the gap plane width to the cylinder diameter, vortex shedding has been largely controlled [15]. The purpose of these researches was to compare and investigate the coefficients of drag and lift on a circular cylinder, to control the flow fluctuations and heat transfer around the circular cylinder. According to [5, 16, 17] lift and drag coefficients are influenced by the movement of particles in a viscous fluid, and the force due to pressure difference acting on the cylinder consists of two components: one from drag force and the other from boundary layer shear

force. It was also observed that at Reynolds numbers of 100 and 500, the drag coefficient accounts for 69% and 83.76% of the total force due to pressure difference [4]. In the studies conducted around the circular cylinder close to the wall, the researchers found that when a circular cylinder moves near a stationary wall in a stagnant fluid, there is no boundary layer effect and only a row of vortices is observed, forming a two-row street-like pattern behind the cylinder [13]. The results indicate that in the case of a cylinder near a stationary wall and a steady flow, if the gap between the wall and the circular cylinder is significantly reduced, counter-clockwise vortices are suppressed by the boundary layer shear flow near the wall and only a single periodic vortex is created downstream [18, 19]. According to [13, 16, 20, 21], The results showed that the boundary layer near the wall is strongly dependent on the velocity gradient of the flow. Therefore, the effects of the gap size between the circular cylinder and the wall on the forces acting on the cylinder and the vortex shedding frequency have been studied and results indicated that for Reynolds numbers greater than 1200, the critical gap between the cylinder and the wall is in the range of 0.2-0.4 D. In this gap, the drag coefficient increases significantly. According to [13], the critical Strouhal number for three Reynolds numbers of 100, 140 and 180 was observed near the moving wall for a gap of 0.6. These studies demonstrated that as the cylinder approaches the wall, intense interactions between vortices and the wall boundary layer occur, leading to an increase in vortex shedding frequency [22]. Additionally, in [7], critical Reynolds numbers were studied in the range of 80-1000, showing that up to Reynolds 1000, the flow exhibits similar behavior. Numerous studies have been carried out to elucidate the dependency of forces acting on a circular cylinder and the vortex shedding frequency. Furthermore, studies have been explored the heat transfer characteristics around a cylinder affected by vortex shedding. Many studies have been conducted in the area of frequency amplification or attenuation of systems in the vicinity of high-speed fluid. In the study of [23], the effect of fluid flow speed on time response was studied and according to this study, the frequency of the system decreased with increasing fluid flow speed. At higher values of fluid flow velocity, the frequency increased to a greater extent. Molochnikov et al. [24] obtained the distributions of local heat transfer coefficients over the cylinder surface as a function of frequency. Park et al. [25] conducted numerical simulations on the unsteady flow around a circular cylinder up to a Reynolds number of 160. The results showed that with an increase in Reynolds number, turbulence presence in the flow improved and heat transfer increased [25]. Further, in the [13], within the Reynolds range of 100-400, it was observed that at the front of the cylinder, the thermal boundary layer is thinnest.

The isothermal lines converge toward the back of the heated cylinder and take on a concentrated, extended form as the Reynolds number rises [4, 13, 20]. In numerous investigations, it has been documented that there is an inverse relationship between the thermal boundary layer's thickness and the local Nusselt number. Additionally, the smallest local Nusselt number may be found where the thermal boundary layer reaches its greatest thickness [26]. Also, it has been observed that with an increase in Reynolds number, the shedding of vortices affects the local Nusselt number, increasing with an increase in Reynolds number, as convection improves with increasing Reynolds number [20, 27, 28]. As it can be concluded in the research [29, 30], the increase in fluid speed is strongly related to the increase in heat transfer improvement. Also, flow characteristics and heat transfer features were simulated [31] by using the finite volume method. The effects of increasing Reynolds number and varying blockage ratios (5, 10, and 112) on different flow and heat transfer attributes were investigated. It was concluded that Reynolds number has the most significant impact on input attribute. Prior work primarily examines fluid dynamics surrounding a

solitary wall and a singular circular cylinder; however, uncertainty remains regarding the impact of neighboring parallel walls on such flows. Researchers have tended to concentrate on individual parameters or situations rather than comparing confined and unconfined cylinder scenarios. Given that adjacent walls increase turbulence in fluids flowing past circular cylinders, further investigation into these particular circumstances is warranted. This will contribute significantly to our understanding of complex fluid-structure interactions under various geometric constraints. Investigating heat losses and flow fluctuations within the range of oil transmission lines is the main motivation for this research. The results of these simulations can be effective in selecting appropriate heating and thermal insulation systems for oil and gas transmission lines in the advancing oil industry. For this purpose, flow characteristics around circular cylinders have been studied and compared for different cases including: far from two stationary walls, a circular cylinder close to a stationary wall, a circular cylinder close to one moving wall, circular cylinder between two walls (both stationary), circular cylinder between two walls (both moving) and circular cylinder between two walls (one stationary and one moving), studied and compared. This study involves comparing and extracting parameters such as lift and drag coefficients, Nusselt and Strouhal numbers for six different cases, focusing on the fluid dynamics and heat transfer aspects of the problem. This includes the confinement of a cylinder between two walls under three different wall speed conditions, which is among the innovations of this research.

The flow around the cylinder is one of the important issues in various engineering fields. Today, with the advancement of technology and the development of new heat exchangers, submarine projectiles near large ships, the movement of high-speed trains inside tunnels, etc., heat transfer in the cylinder near the moving wall has become more important.

Building upon prior work, the current investigation expands on the role of differing wall velocities influencing the flow patterns around a circular cylinder situated between two closely abutted vertical partitions. Notably, this configuration impacts flow oscillations and generates heightened heat dissipation emanating from the cylindrical entity. Confirmatory evidence supports amplified vortex formation accompanied by intensified fluctuation levels in the lift and drag coefficients. Essential methodological details, including selection of governing differential equations, resolution techniques, and verification procedures occupy Section 2 of the manuscript. Section 3 proceeds to detail outcomes derived from five separate simulation scenarios: Fixed Stationary Walls (FSW); Nearly Stationary Wall - Scenario 1 (NSW-1, gap=2D); Non-Moving Wall - Scenario 1 (NMW-1, gap=2D); Nearly Stationary Wall - Scenario 2 (NSW-2, gap=2D); Non-Moving Wall - Scenario 2 (NMW-2, gap=2D); Nearly Stationary & Moving Wall (NS&MW, gap=2D). Finally, Section 4 summarizes key conclusions drawn from the presented research.

2. Numerical Approach

2.1. Governing Equations

In this study, the flow and thermal fields around a circular cylinder in proximity to a wall were simulated using the finite volume method. Consequently, the governing equations for a Newtonian fluid, which characterize the thermal fields, include the Navier-Stokes, Continuity, Momentum and Energy equations. This leads to the derivation of three dimensionless parameters: Reynolds, Prandtl and Strouhal numbers. Similarly, the dimensionless surface and time-averaged Nusselt number is computed from the time-averaged total heat transfer graph.

$$\frac{\partial u_i}{\partial t} + \frac{\partial u_i u_j}{\partial x_j} = -\frac{\partial p}{\partial x_i} + \frac{1}{Re} \frac{\partial^2 u_i}{\partial x_j^2} + f_i \tag{1}$$

$$\frac{\partial u_i}{\partial x_i} = 0 \tag{2}$$

$$\frac{\partial T}{\partial t} + \frac{\partial u_i T}{\partial x_j} = \frac{1}{Re Pr} \frac{\partial^2 T}{\partial x_j^2} + h \tag{3}$$

$$Re = \frac{\rho \mu D}{k} \tag{4}$$

$$Pr = \frac{c_p \mu}{k} \tag{5}$$

$$Nu = \frac{q_{total}}{A(T_s - T_{flow})} \tag{6}$$

$$st = \frac{1}{t_l u} \tag{7}$$

Where, x_i are Cartesian coordinates, u_i are the corresponding velocity components, t is the time, p is the pressure, and T is the temperature. The momentum forcing f_i is applied on the body surface. μ indicates viscosity, c_p heat capacity especially at constant pressure, k is the conductive heat transfer coefficient and the heat source/sink h is applied to satisfy the iso-thermal boundary condition. t_l is the lift coefficient fluctuation period and q_{total} is the average of the total heat transferred from the cylinder, which is extracted from diagram total heat transfer after stabilization. The symbols ρ , D , t , h , Pr , T_s , and T_{flow} represent density, cylinder diameter, time, convective heat transfer coefficient, Prandtl number, surface temperature of the cylinder, and fluid temperature, respectively. In this research, constant Prandtl number equal to 0.7, which corresponds to air and Reynolds numbers with values of $Re = 100, 140, 180, 200$ have been considered. Following flowchart, include the divisions and boundary conditions of the present studies (*Figure 1*).

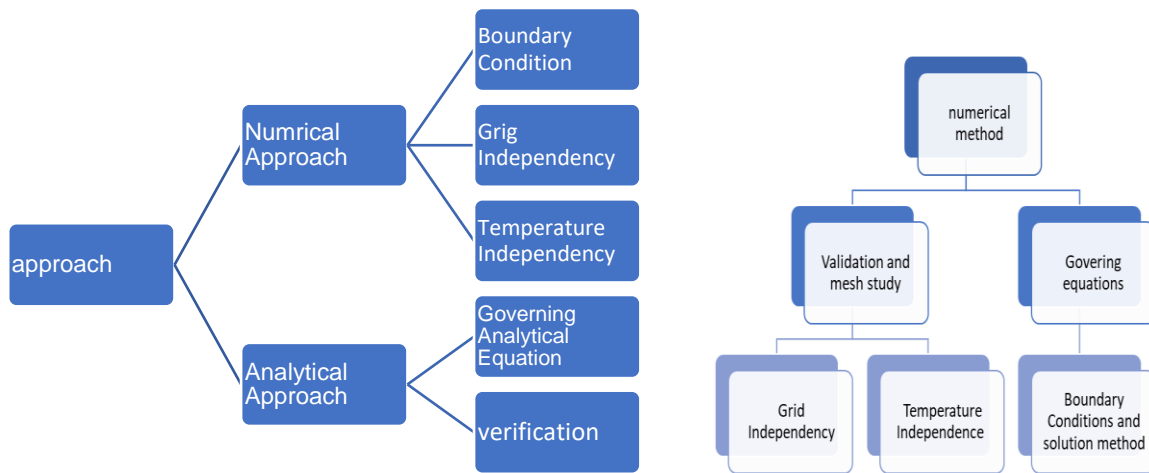


Figure 1. flowchart, including divisions and boundary conditions.

As it shown in the *Figure 1*, numerical method is classified as validation (including Grid independency, temperature independency) and governing equation (boundary condition and solution method).

2.1.1. Boundary Conditions

During this research, a uniform-velocity input boundary setting was prescribed, assuming a motionless circular cylinder and adopting the no-slip principle along the cylinder and contacting sidewalls. By applying these preconditions, a controlled environment was established to facilitate the detailed examination of the targeted hydrodynamic interactions. For the outflow boundary, considering the incompressibility of the fluid and absence of pressure input values, an outflow boundary condition was employed. The fluid temperature was set at 300 K. The specific boundary conditions utilized in this simulation varied depending on the state of the cylinder and walls, as detailed in **Table 1**. To conduct this research, an HP laptop 15-da 2xxx with a dual-core 10510U CPU and 8 GB of RAM was used. The average runtime was 6 hours, although in some high load cases, the CPU runtime reached up to 8 hours. This investigation was conducted using the finite volume method, and the problem is formulated as a pressure-based problem using the pressure changes within a bounded volume and the Navier-Stokes equations to solve the problem using the Simple algorithm and second order discretization. The Simple algorithm and second-order discretization method were employed to solve the Navier-Stokes equations in fluid dynamics. Initially, the Navier-Stokes equations were solved simultaneously within a defined volume using the finite volume method. Subsequently, employing the second-order discretization method, changes in fluid properties such as pressure and temperature within the flow were considered. It enables accurate assessment of fluid properties and flow characteristics at various locations within the volume. **Figure 2** illustrates the computational domain and meshing around a circular cylinder near the wall. The computational domain spans $-50D < x < 50D$ and $0 < y < 50D$. The total number of grid points in the overall geometry is 160,000, with 80,000 grid points allocated around the circular cylinder within a $4 \times 4D$ square. To address this matter, the computational domain was partitioned into 12 sections utilizing a non-uniform hyperbolic grid. This gridding approach facilitates finer grid resolution around the cylinder and adjacent to the wall. **Figure 2** provides a magnified view of the meshing surrounding the cylinder.

In the course of the simulation process, equilibrium in terms of stable and recurring flow and thermal undulations was accomplished roughly after clocking up 600 time units. Through the calculation and subsequent averaging of graphical depictions representing lift and drag coefficients alongside aggregate heat transfer metrics, the respective Nusselt and Strouhal figures were accurately extracted for Re numbers encompassing 100, 140, 180, and 200. Further elaboration reveals that the designated inlet airspeeds correspond to 0.1 m/s for Re 100, 0.14 m/s for Re 140, 0.18 m/s for Re 180, and finally culminating in 0.2 m/s specifically for Re 200. It should be noted that precision in language has been preserved to ensure accurate representation of quantitative relationships in conjunction with appropriate referencing style suitable for academic papers. Additionally, minor adjustments have been made to phraseology to enhance cohesiveness and promote improved reading experience.

Table 1. Boundary conditions for 6 different investigated situations. The number 1 in the abbreviation names is used when the cylinder is close to one of the walls and the number 2 is used when it is close to both walls.

	velocity inlet	Cylinder surface temperature	Upper wall velocity	Bottom wall velocity
FSW	$u = U$ $v = 0$	500 (k)	$V = 0$	$V = 0$
NSW-1	$u = U$ $v = 0$	500 (k)	$V = 0$	$V = 0$
NMW-1	$u = U$ $v = 0$	500 (k)	$U/V = 1$	$V = 0$
NSW-2	$u = U$ $v = 0$	500 (k)	$V = 0$	$V = 0$
NMW-2	$u = U$ $v = 0$	500 (k)	$U/V = 1$	$U/V = 1$
NS&MW	$u = U$ $v = 0$	500 (k)	$U/V = 1$	$V = 0$

As displayed in **Table 2** of the current investigation, the attained numerical outcomes have been juxtaposed against relevant preceding scholarship focusing on unrestricted circular cylinders [13, 29-32]. Gratifying consistency was detected between the findings reported in the present study and earlier published works, affirming the validity of the employed computational approaches and models. To maintain conciseness and alignment with typical conventions in scientific writing, the description has been condensed while still emphasizing the favorable correlation between the investigated research and previously documented literature. Slight modifications in word choice contribute to a more streamlined narrative, ensuring continued focus on the comparison of the results.

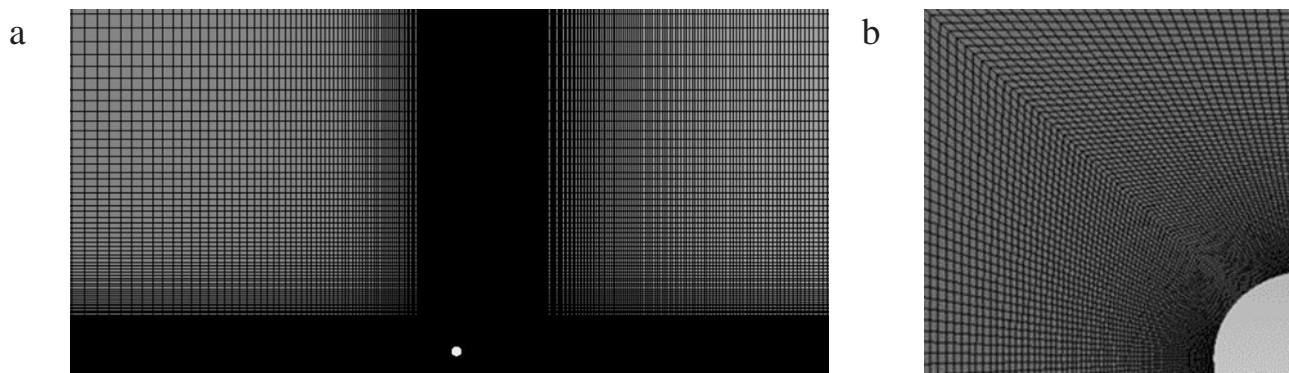


Figure 2. Mesh structure in the computational area, a) A general view of the mesh, b) zoom of the area around the cylinder

2.2. Validation and Mesh Study

In this study, the validation and thermal independence of the problem from temperature and grid resolution have been examined. Furthermore, a comparison is presented in **Table 2**. In **Table 2**, efforts have been made to determine the optimal grid resolution by increasing the number of grid points surrounding the cylinder. The values in the table represent the number of grid points around

the circular cylinder. Based on **Table 2**, an optimal grid resolution of 80,000 has been chosen for the current research problem. Also, as the temperature of the cylinder surface increases, the overall heat transfer also increases. Therefore, it is crucial to establish temperature independence to determine the cylinder temperature accurately. Based on **Table 2**, we confirm the independence of the parameters utilized in the current problem from temperature. The results of global flow parameters (*St*, *Cd* ave, *Cl* rms and *Nu*) are listed in **Table 3** along with the available data. A satisfactory agreement between the present results and the previous numerical as well as experimental studies is obtained. In **Figure 3**, a comparison of the Strouhal number for the FSW case is provided with two references. As evident in the figure, at Reynolds 100, the results of the current paper differ significantly from the references. However, as the Reynolds number increases, this difference decreases and becomes negligible. The FSW case simulated in this study is not completely unbounded and is located at a very large distance from the two walls, hence this difference is observed.

Table 2: Numerical results independent from the mesh size and quantity.

	number of grids	Cd_{ave}	Cl_{ave}	Cl_{ave} Changes	Cd_{ave} Changes
Mesh study	10,000	1.398	0.0382	-	-
(Re 180)	20,000	1.375	0.0385	1,6%	0.65%
	40,000	1.371	0.0397	0.39%	3.16%
	80,000	1.359	0.0387	0.80%	2.4%
	160,000	1.358	0.0386	0.041%	0.44%
surface and time		600(k)		500(k)	400(k)
average		5.156		5.156	5.155
Nusselt number					
(Re 100)					

Table 3: Comparison of flow parameters at Re = 200.

	Cl_{rms}	Cd_{ave}	Nu	St
Present study	0.482	1.383	7.482	0.194
Cheng et al.[32]	-	1.312	7.5	0.19
Yoon et al.[13]	0.48	1.32	7.3	0.194
Ding et al.[33]	0.467	1.35	-	0.196
Alam et al.[34]	0.49	0.140	-	0.195
Mahír and Altaç [35]	0.494	1.376	7.474	0.192

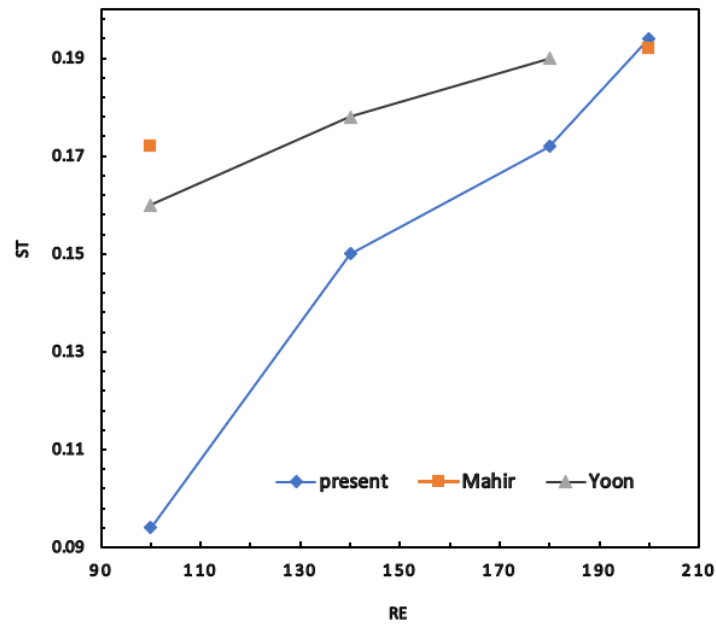


Figure 1. comparisons of the present study and references for the case of an unbounded circular cylinder

3. Results and Discussions

3.1. Flow Dynamics Analysis

In this section, we have investigated the flow parameters, contours and velocity profiles around a circular cylinder for six different cases. In this range of Reynolds numbers and under these conditions, vortex shedding behind the cylinder has occurred. In this section, we have attempted to examine the effect of the presence of the moving and stationary wall on fluid parameters and the shape of the vortex shedding. *Figure 4* displays the velocity distribution for a circular cylinder away from walls at four different Reynolds numbers (100, 140, 180, 200). Figure depictions reveal heightened fluid speeds adjacent to the cylindrical surface compared to the general flow rate, subsequently inducing vortex shedding. Specifically, two separate vortex sequences materialize downstream from the cylinder - one featuring clockwise rotation originating above, and another counterclockwise motion emerging beneath. Notably, these phenomena significantly affect hydrodynamic pressures exerted on the cylindrical component along with influencing the underlying convective heat transmission process implicated during the liquid-solid interface interaction. The visualization in *Figure 4* indicates that vortex shedding becomes more prominent as Reynolds number increases. Additionally, the number of vortices behind the cylinder grows and vortex lines become denser and more concentrated. *Figure 5* illustrates the impact of a stationary wall's boundary layer on vortex shedding. The lower row of vortices significantly interacts with the wall's boundary layer, resulting in their combination. Consequently, a region of very low velocity is formed within the wall's boundary layer. As Reynolds number increases, the influence of the boundary layer on the upper row vortices diminishes and these vortices are thrown in a direction towards the boundary layer.

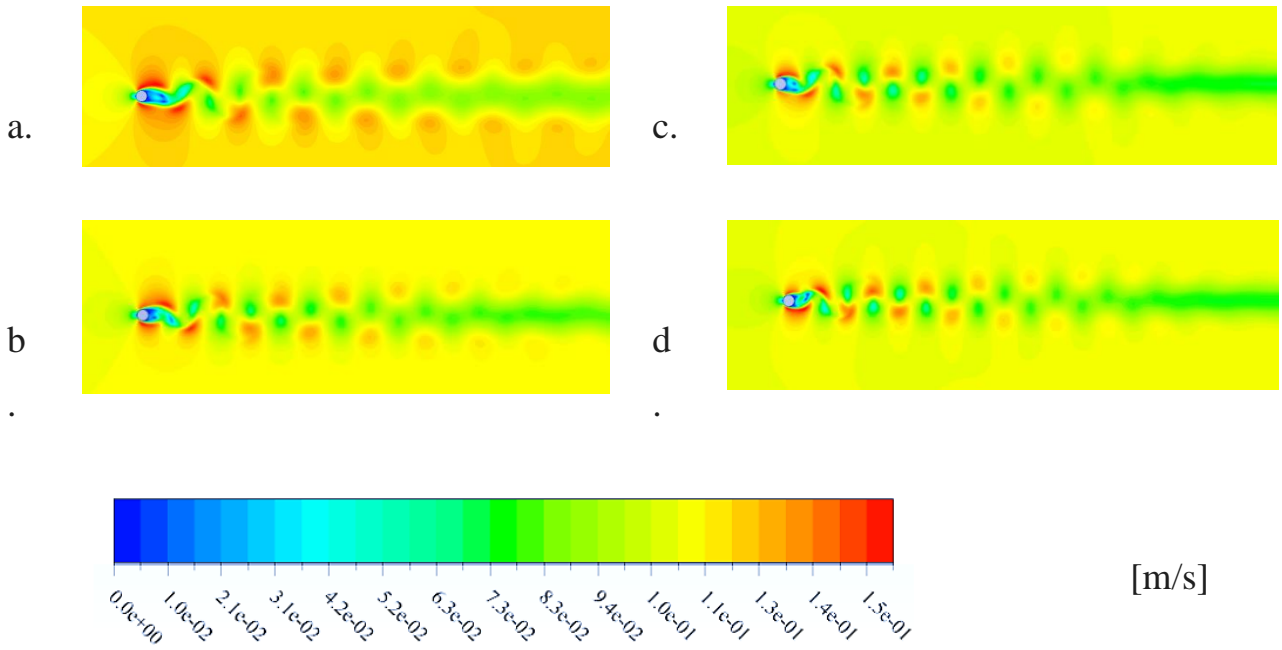


Figure 4. Velocity contours for the FSW case at various Reynolds numbers (a) 100, (b) 140, (c) 180, (d) 200

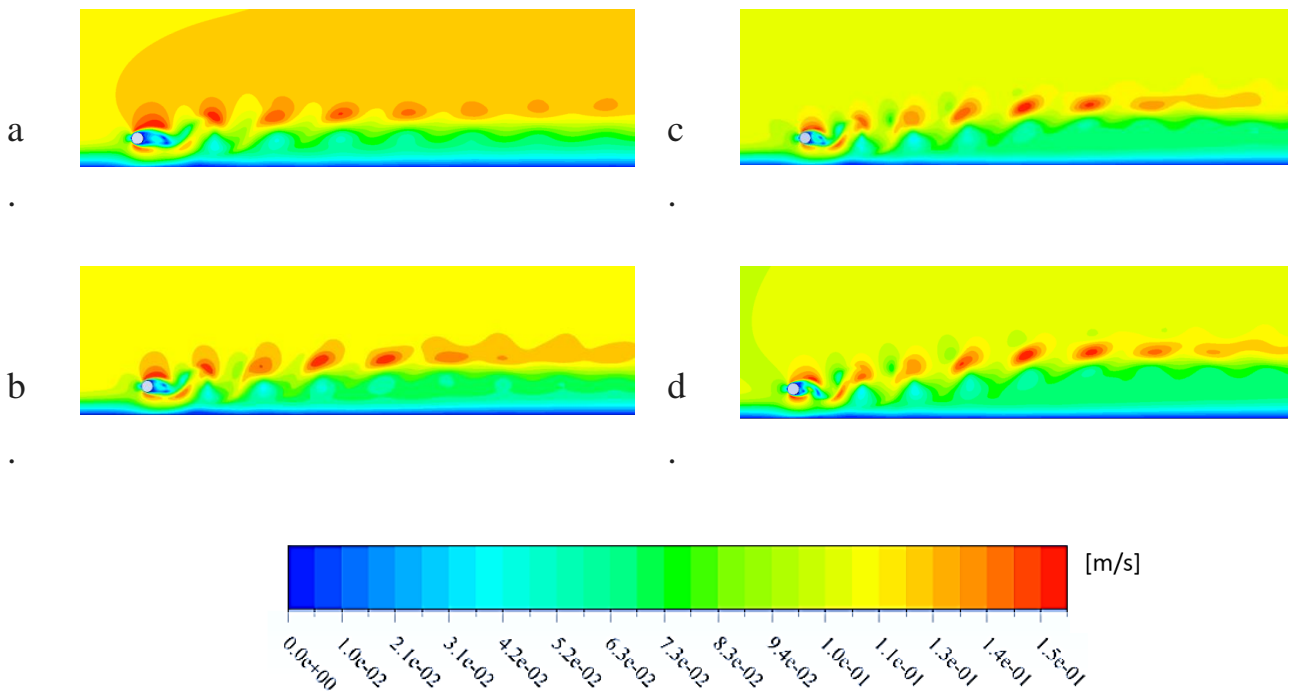


Figure 5. Velocity contours for the NSW-1 case at various Reynolds numbers (a) 100, (b) 140, (c) 180, (d) 200.

In the scenario of a circular cylinder near a moving wall, it is assumed that the wall's velocity matches that of the fluid. **Figure 6** demonstrates the absence of a boundary layer on the wall, with two distinct rows of vortices forming behind the cylinder. The overall shape of these vortices

resembles the configuration far from two walls. As can be seen in **Figures 7-9**, by positioning a circular cylinder between two walls, reducing the flow's cross-sectional area and adhering to the continuity equation, fluid velocity significantly increases around the cylinder. As shown in the figures, the motion of walls significantly aids in the stability of vortices. In the case where the cylinder is between two stationary walls, in all Reynolds numbers, as depicted in **Figure 7**, the upper row of vortices strongly interacts with the upper wall's boundary layer, while the lower row interacts with the bottom wall's boundary layer. This interaction results in lower velocity regions within the boundary layers due to the merging of wall boundary layers and vortices. The high-speed regions between vortices are closely spaced and form a continuous, fluctuating line in the region behind the circular cylinder. As illustrated in **Figure 8**, when the walls move parallel to the flow direction at the same velocity as the fluid, no boundary layer is present on the walls. The movement of walls has caused the flow to become laminar near the walls. Additionally, with increasing Reynolds number, the frequency of vortex shedding and the number of vortices in each row have increased and two distinct rows of vortices form behind the circular cylinder. Based on **Figures 4-9**, it can be inferred that for this case, with an increase in Reynolds number, the density of vortex lines has increased and in the NMW-1 and NMW-2 cases, under the influence of wall motion, vortices have moved away from the walls. In cases NSW-2 and NSW-1, the vortices have been damped faster, while in cases NMW-2 and NMW-1, the vortices remain stable and pass through the flow. In the case of a cylinder near two walls (one stationary and one moving), similar conditions are observed for the bottom and top walls compared to the NSW-2 and NMW-2 cases. Vortices from the lower row combine with the bottom wall's boundary layer, creating a low-speed region with a slight curvature behind the cylinder. The upper vortex row is deviated from the distance between the two rows due to the curvature of the boundary layer. Due to the low pressure of the area near the moving wall, the upper vortex line is formed on the moving wall. Analysis of drag and lift coefficients for a circular cylinder situated far from a wall indicates an increase with rising Reynolds number and fluid velocity, as observed in **Figure 10**. For a cylinder positioned far from walls and in close proximity to a stationary wall, the drag and lift coefficients remain consistent across at the four Reynolds numbers compared. Variations are notable at lower Reynolds due to increased interference of vortices with the lower wall's boundary layer. In the scenario of a circular cylinder near a moving wall, drag and lift coefficients increase at Reynolds 100 and 140 compared to the previous cases. However, at Reynolds 180, a decrease in drag coefficient is observed. At Reynolds 200, there is a marginal increase of 0.7%. Consequently, the impact of stationary or moving walls on drag coefficient is more pronounced at Reynolds 100, diminishing significantly at Reynolds 200 due to the predominant effect of increased fluid velocity.

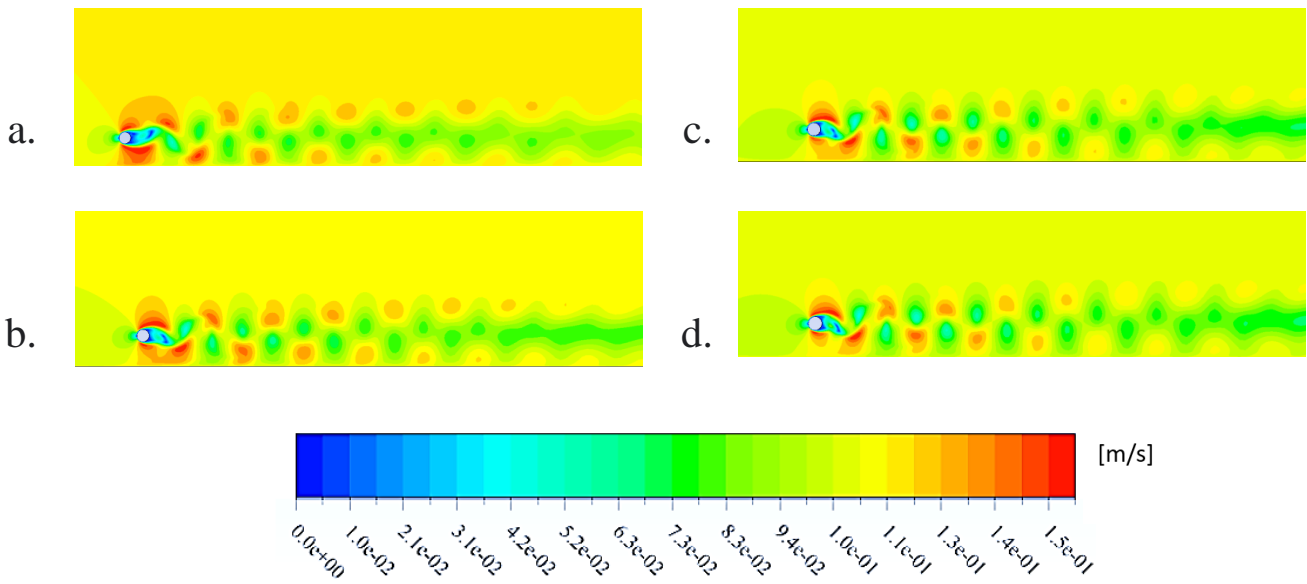


Figure 6. Velocity contours for the NMW-1 case at various Reynolds numbers (a) 100, (b) 140, (c) 180, (d) 200.

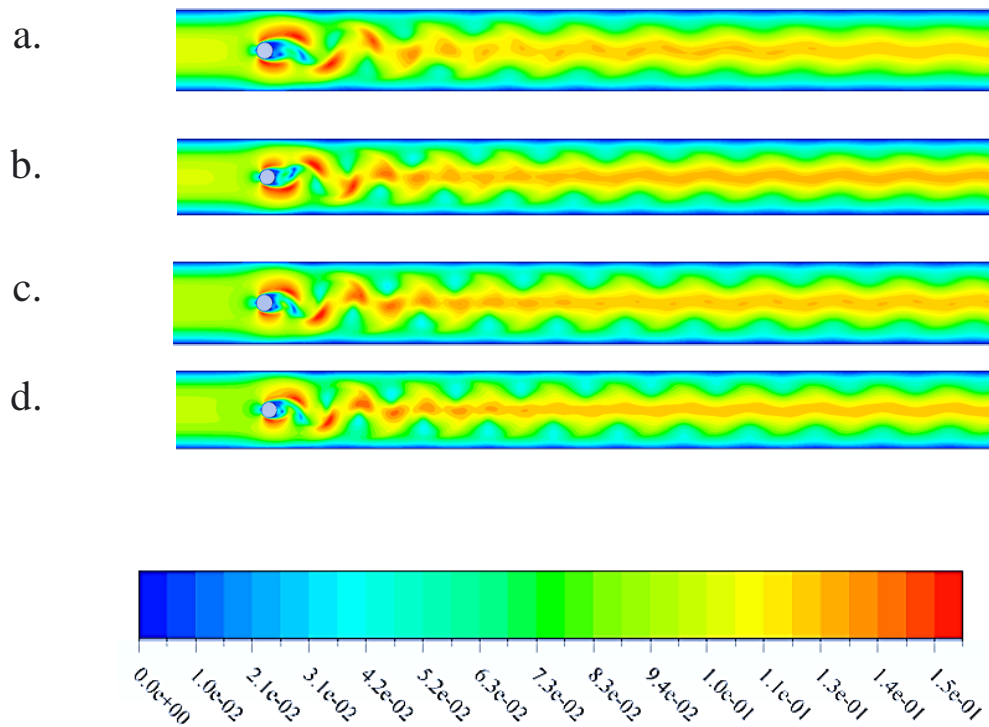


Figure 7. Velocity contours for the NSW-2 case at various Reynolds numbers: (a) 100, (b) 140, (c) 180, (d) 200.

By comparing **Figures 6 and 7**, it is clear that the walls accelerate the damping of vortices. Also, the maximum speed is higher in the case where both walls are near the cylinder compared to the case where only one wall is near the cylinder.

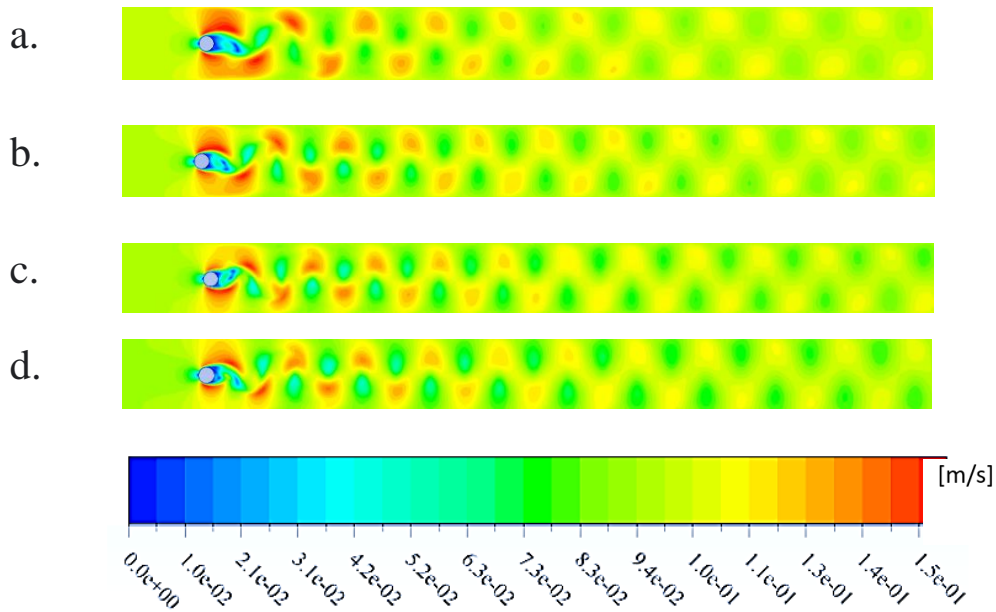


Figure 8. Velocity contours for the NMW-2 case at various Reynolds numbers: (a) 100, (b) 140, (c) 180, (d) 200.

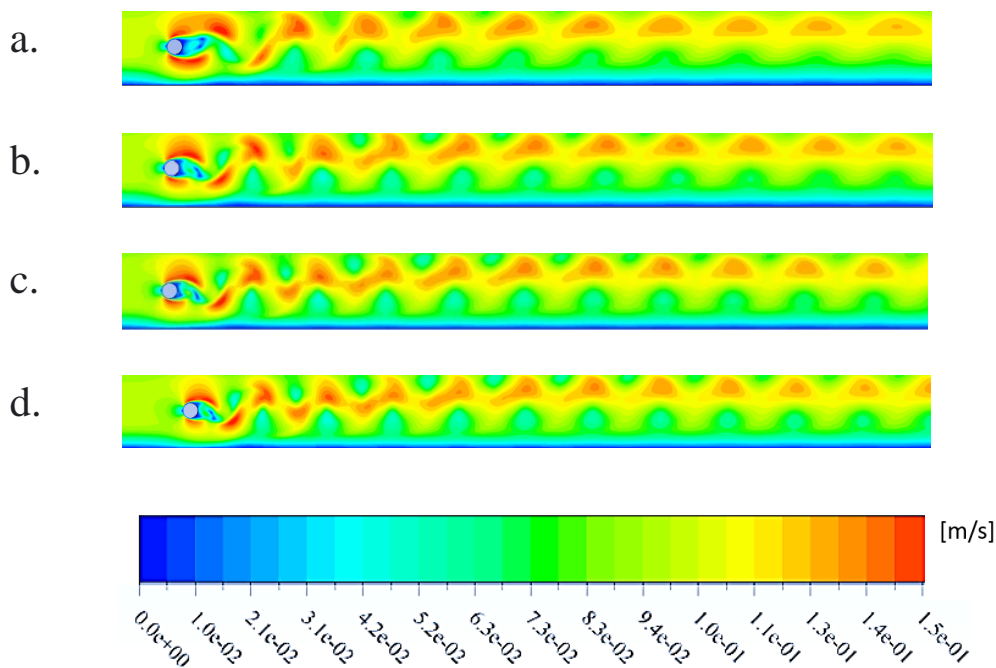


Figure 9. Velocity contours for the NS&MW case at various Reynolds numbers: (a) 100, (b) 140, (c) 180, (d) 200.

Comparing **Figures 8 and 9**, it is clear that the moving wall has a much smaller effect on the formation of the boundary layer and also causes less damping in the vortices compared to the stationary wall. Analysis of **Figure 10** reveals a substantial increase in velocity by presences two walls near the cylinder in all three scenarios. An escalation in velocity precipitates substantial surges in both lift and drag coefficients, especially noticeable when a cylinder resides amidst immobile parallel walls. Under these circumstances, intensified frictional resistance amongst successive flow strata, correlating with amplifying Reynolds numbers, eventually causes

diminished net fluid speed. Consequently, augmented frictional force hindrance acts upon the encompassing viscous fluid, thereby affecting the cylinder's exposure to fluid pressure and subsequent interactive heat transmission capacities. The influence of friction and speed reduction on drag coefficient is clearly demonstrated in *Figure 10*.

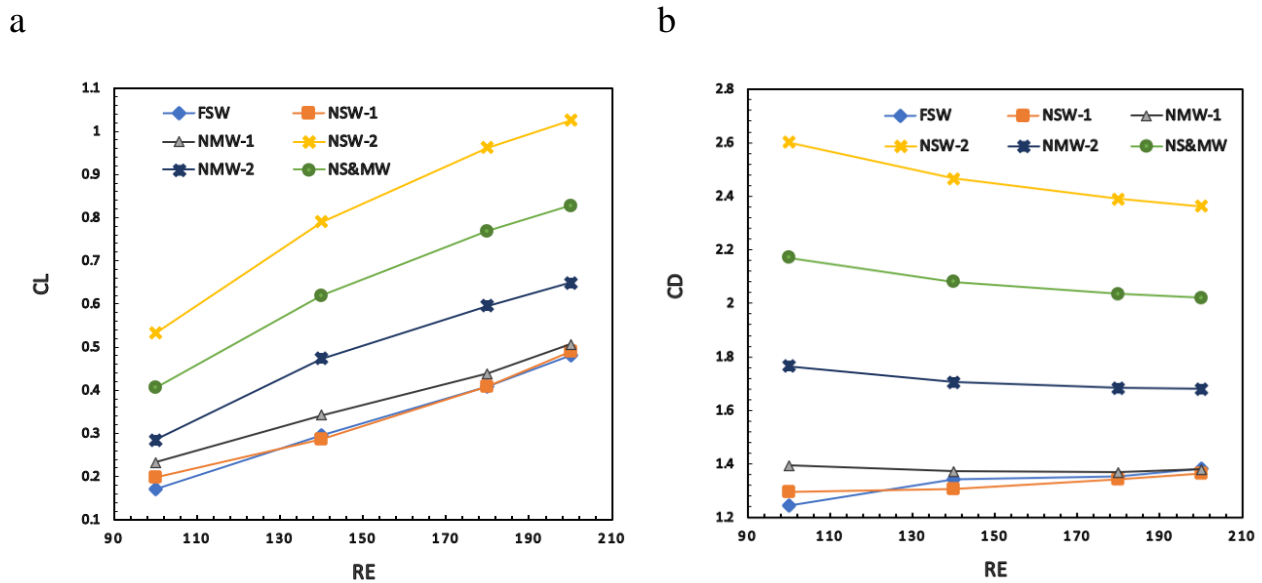


Figure 10. a) Lift coefficient and b) drag coefficient as a function of Reynolds number at four different Reynolds numbers of 100, 140, 180 and 200.

According to *Figure 8*, in the scenario where a cylinder is positioned between two moving walls, the movement of the walls contributes to the laminar flow and deceleration around the cylinder, resulting in a smaller increase in drag and lift coefficient values compared to the previous state. Undoubtedly, greater vortex oscillations correspond to higher lift coefficients. When contemplating a circular cylinder flanked by a static and a moving wall, we discern a decline in drag coefficient associated with rising Reynolds numbers, analogous to prior instances. Moreover, the lift coefficient ascends proportionately alongside enhanced fluid velocity. Thus, this unique configuration demonstrates partial parallels with preceding ones yet maintains distinctiveness; henceforth, the relevant lift and drag coefficients fall within the range spanned by earlier established benchmarks. According to *Figure 11*, The Strouhal number increases with Reynolds number due to enhanced vortex shedding and flow fluctuations. The presence of stationary or moving wall had a significant effect on the Strouhal number. As can be seen in *Figure 11*, the Strouhal number has increased in all cases with the increase of Reynolds number. Also, the critical Strouhal number for mode m was observed at Reynolds 200.

Physically, the closer the walls are to the cylinder, the smaller the distance of the vortices from the cylinder becomes, which means that the cylinder experiences more lift and drag forces. In addition, the movement of the wall reduces the boundary layer and thus more space for the formation of vortices, which reduces the lift and drag forces are reduced.

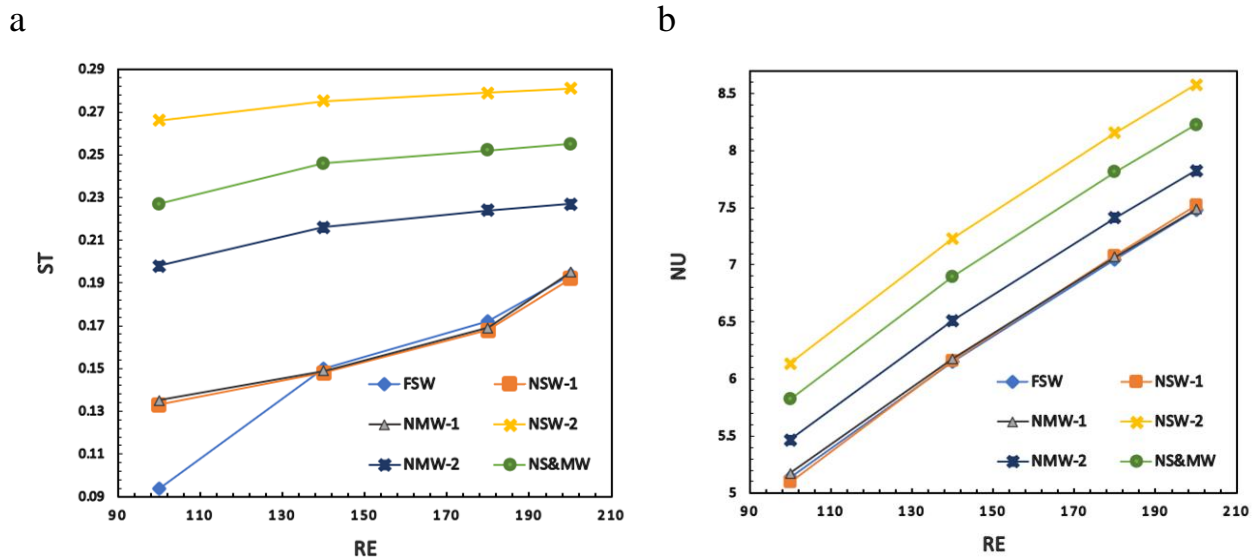


Figure 11. a) Strouhal number and b) time and surface average Nusselt number as a function of Reynolds number at four different Reynolds numbers of 100, 140, 180 and 200.

3.2. Heat transfer

Temperature contours for six different positions of the cylinder relative to walls are shown in *Figures 12-17*. Heat transfer behavior varies across these models based on temperature distribution, flow characteristics and wall proximity. The density of isothermal lines under the influence of two vortex rows is illustrated in *Figure 12*. Heat transfer and Nusselt number are highly influenced by turbulence and flow speed, as depicted in *Figure 11*. Hence, as depicted in *Figure 11*, the time-averaged and surface-averaged Nusselt number increases with rising Reynolds number, fluid velocity and vortex fluctuations. In the case of a cylinder positioned near two stationary, moving, or combined walls, as illustrated in *Figures 4-9* and diagram in *Figure 11*, the increase in Reynolds number leads to heightened turbulence and friction between flow layers. Consequently, the Nusselt number for these configurations exhibits a greater increase compared to previous scenarios. As evident in *Figures 12-17*, in all six mentioned cases, with an increase in Reynolds number, the thermal boundary layer thickness decreases. Additionally, the minimum thermal boundary layer thickness around the cylinder is observed at the front of the cylinder. According to *Figures 12-17*, the isothermal lines coincide with vortex shedding. Based on *Figure 12*, the boundary layer effect of a stationary wall has caused the temperature contours around the cylinder to be asymmetric relative to the cylinder's central axis.

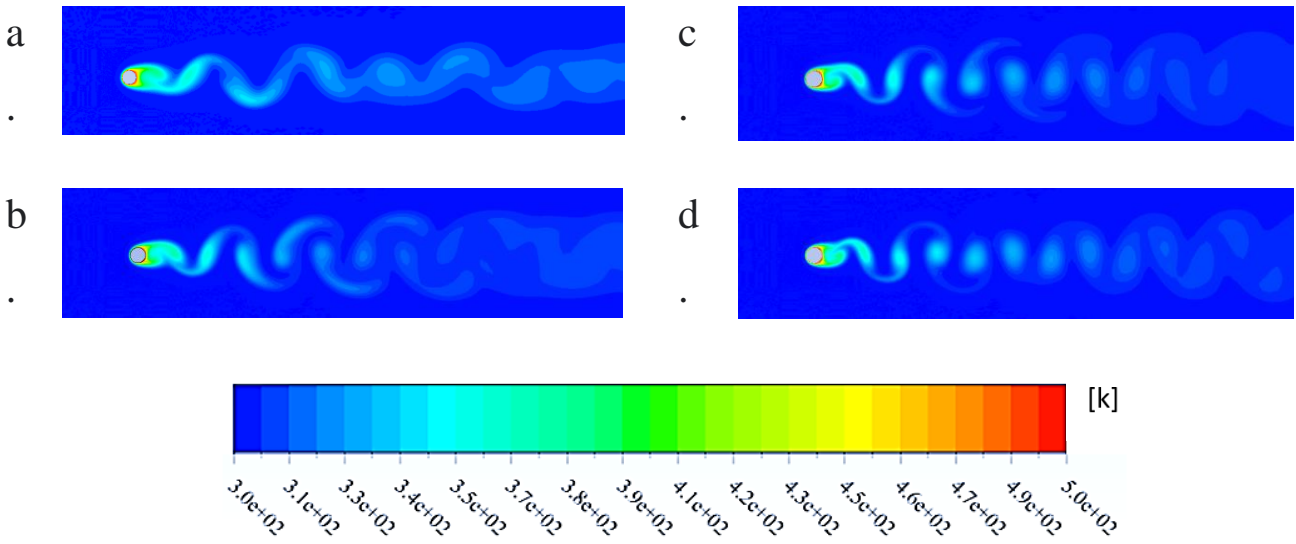


Figure 12. Temperature contours for the FSW case at various Reynolds numbers: (a) 100, (b) 140, (c) 180, (d) 200.

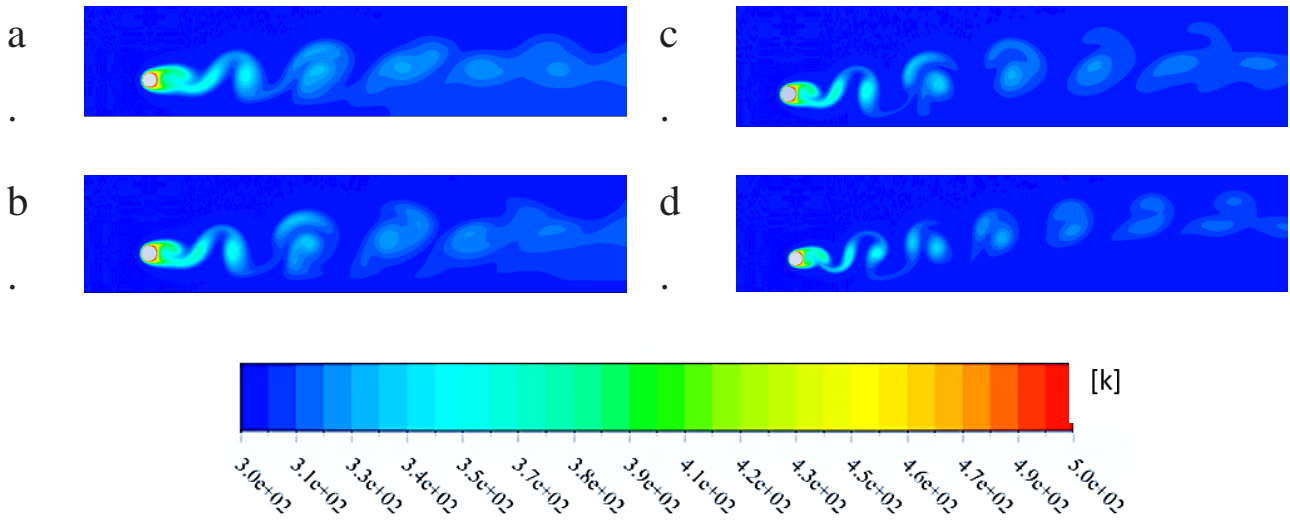


Figure 13. Temperature contours for the NSW-1 case at various Reynolds numbers: (a) 100, (b) 140, (c) 180, (d) 200.

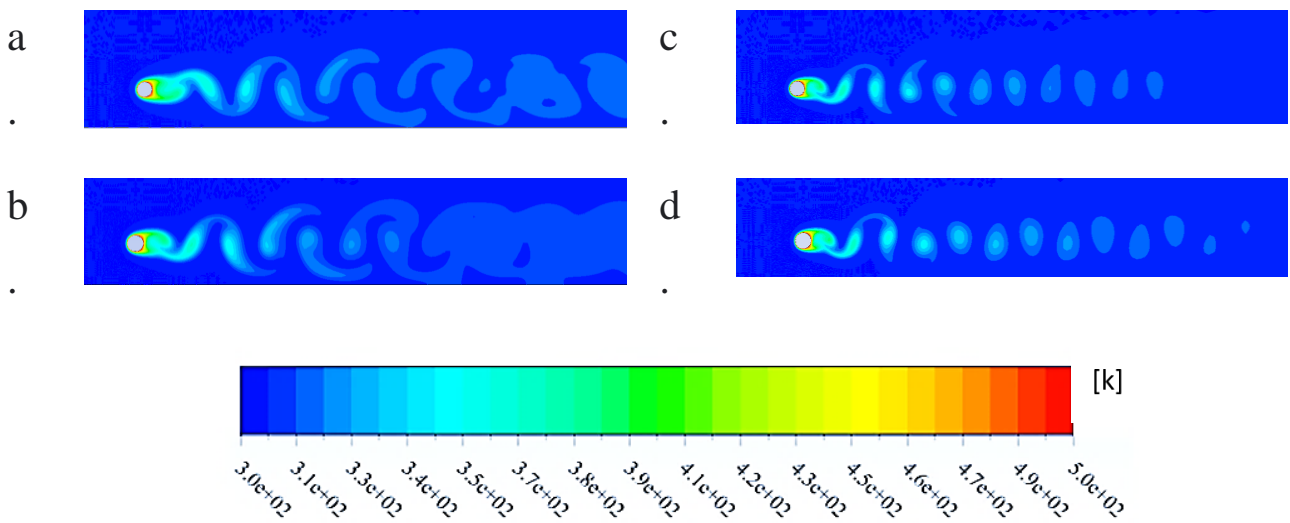


Figure 14. Temperature contours for the NMW-1 case at various Reynolds numbers: (a) 100, (b) 140, (c) 180, (d) 200.

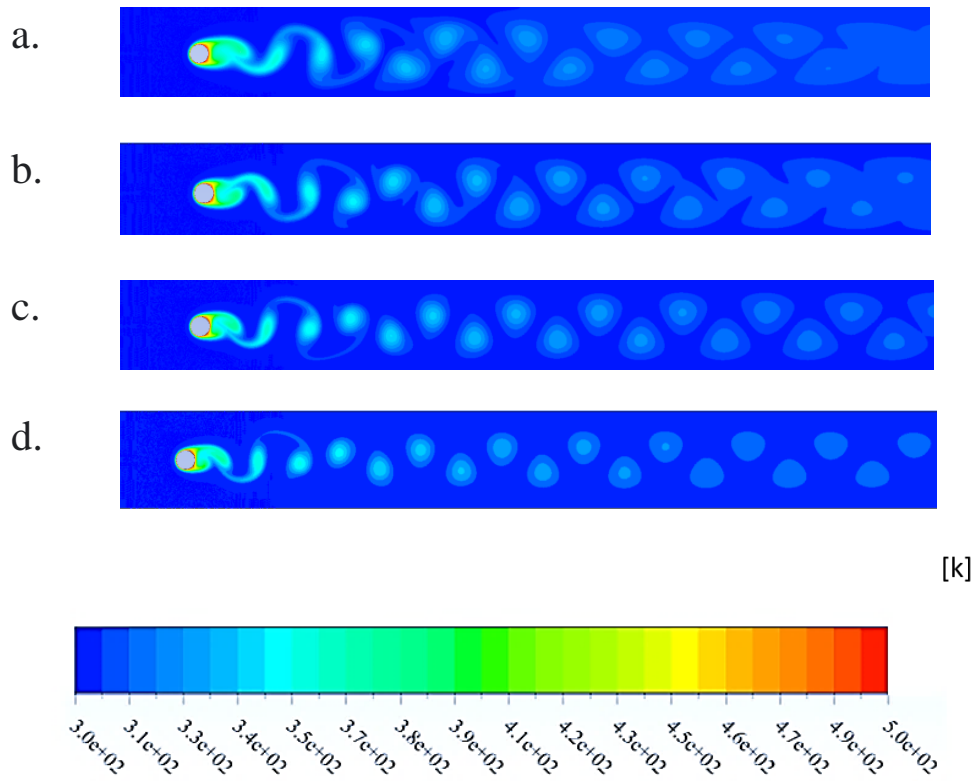


Figure 15. Temperature contours for the NSW-2 case at various Reynolds numbers: (a) 100, (b) 140, (c) 180, (d) 200.

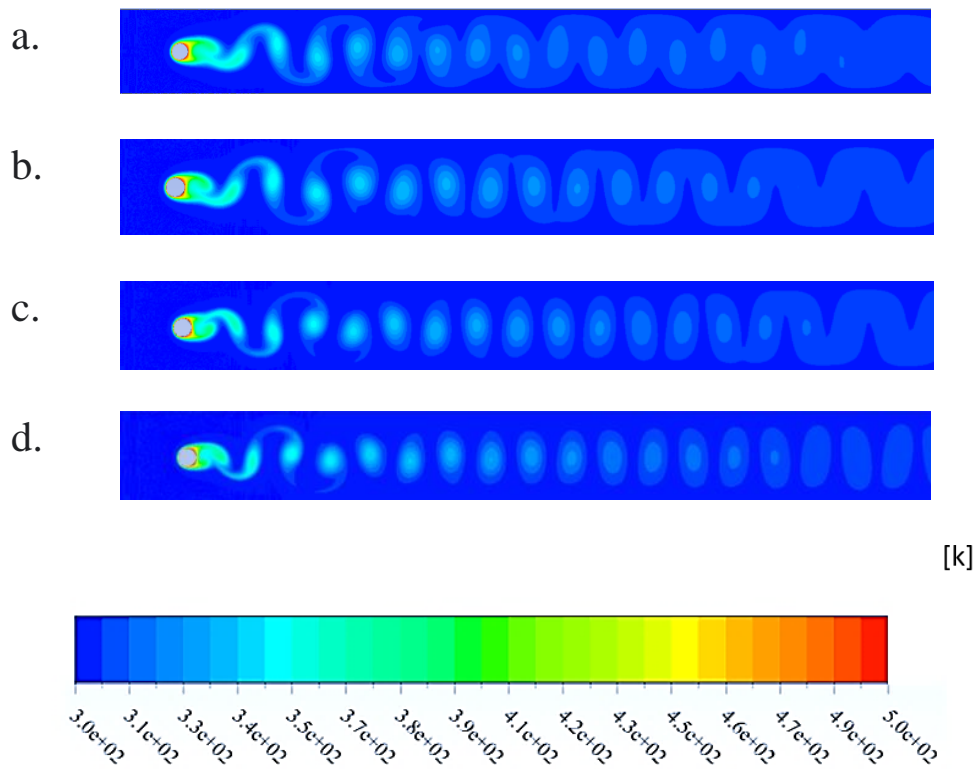


Figure 16. Temperature contours for the NMW-2 case at various Reynolds numbers: (a) 100, (b) 140, (c) 180, (d) 200.

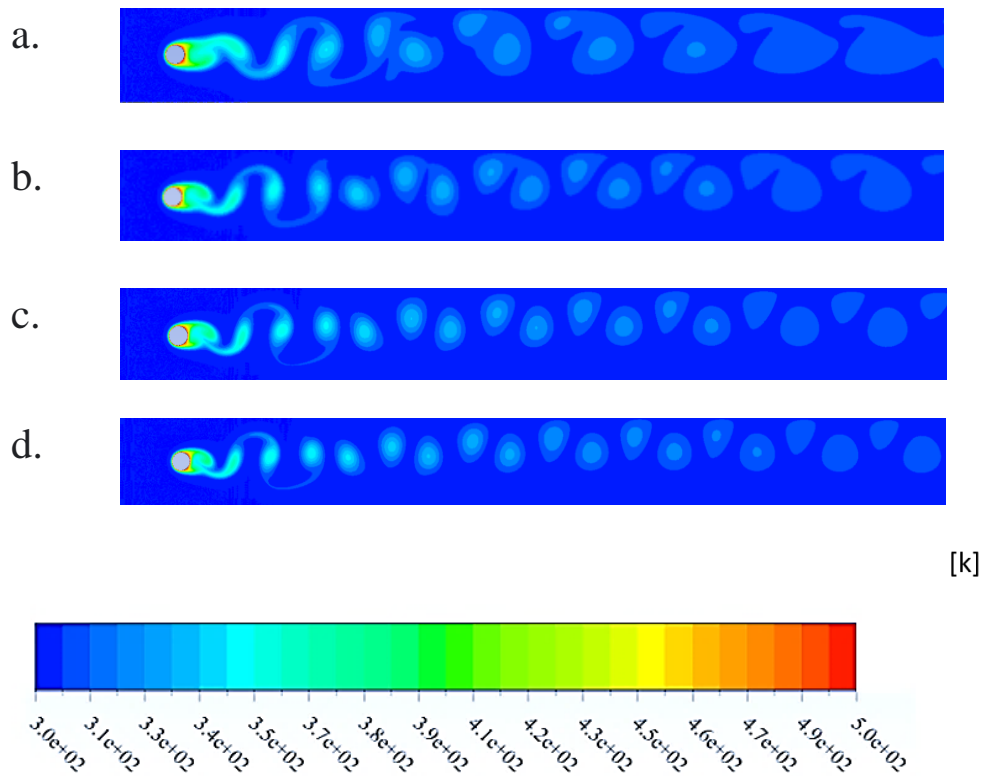


Figure 17. Temperature contours for the NS&MW case at various Reynolds numbers: (a) 100, (b) 140, (c) 180, (d) 200.

According to **Figure 14**, there is elevated heat transfer activity compared to the isolated cylinder situation due to the stabilization of vortices and isotherms facilitated by the wall's movement in States NMW-1, as depicted in **Figures 14 & 6**. To thoroughly examine alterations in vorticity patterns, Isothermal contours serve as useful indicators in States FSW, NSW-1, NSW-2, NMW-1, NMW-2, and NS&MW, as demonstrated in **Figures 15-17**. Particularly notable is State NMW-1, wherein the combined influence of lift force and moving walls draws the vortex pairs closely together and virtually aligned, as displayed in **Figure 16**. For rigorous scrutiny, consult **Table 4** presenting detailed numeric data concerning six distinct states and four varying Re ranges. Complementing graphical representations in **Figures 10 and 11**, this tabular compilation offers a holistic perspective on the intricate temperature distributions governing diverse geometries. Based on the data in the **Table 4**, with an increase in Reynolds number, the highest increase in the Nusselt number was 47% in case NSW-1. Similarly, the highest percentage increases in the lift coefficient, drag coefficient, and Strouhal number were 183%, 111%, and 106%, respectively, observed for the case of FSW. Nevertheless, the highest increase in all parameters under consideration was found in the Strouhal number with a 182% increase, Nusselt number with a 19% increase, lift coefficient with a 212% increase, and drag coefficient with a 108% increase compared to case FSW, in case NSW-2.

As already described, physically, the turbulence increases as the walls get closer to the cylinder, which increases the heat transfer and thus the Nusselt number. As the movement of the walls, the boundary layer also decreases, which reduces the turbulence and the heat transfer also decreases.

Table 4: the numerical results obtained include drag and lift coefficients, Nusselt and Strouhal numbers for six configurations of a cylinder and walls at various Reynolds numbers 100, 140, 180 and 200.

		St	Cl	Cd	Nu
Re = 100	FSW	0.094	0.17	1.245	5.138
	NSW-1	0.133	0.198	1.297	5.099
	NMW-1	0.135	0.233	1.394	5.173
	NSW-2	0.266	0.532	2.602	6.135
	NMW-2	0.198	0.285	1.765	5.476
	NS&MW	0.227	0.406	2.17	5.822
Re = 140	FSW	0.15	0.295	1.341	6.151
	NSW-1	0.148	0.287	1.305	6.155
	NMW-1	0.149	0.343	1.372	6.176
	NSW-2	0.275	0.79	2.465	7.231
	NMW-2	0.216	0.474	1.705	6.514
	NS&MW	0.246	0.619	2.08	6.897
Re = 180	FSW	0.172	0.409	1.352	7.048
	NSW-1	0.168	0.408	1.341	7.081
	NMW-1	0.169	0.439	1.369	7.068
	NSW-2	0.279	0.962	2.389	8.158
	NMW-2	0.224	0.596	1.684	7.412
	NS&MW	0.252	0.769	2.034	7.812
Re = 200	FSW	0.194	0.482	1.383	7.482
	NSW-1	0.192	0.49	1.365	7.519
	NMW-1	0.195	0.506	1.379	7.486
	NSW-2	0.281	1.026	2.362	8.578
	NMW-2	0.227	0.649	1.68	7.824
	NS&MW	0.255	0.828	2.02	8.228

4. Conclusion

In the present study, the flow around the circular cylinder was simulated in six different configurations and the amount of heat transfer from the cylinder to the fluid was extracted in these states. The analysis of drag coefficients indicated that by increasing the Reynolds number, there was an enhancement in the critical drag coefficient across these configurations, leading to a decreasing trend. Furthermore, lift coefficients and Strouhal numbers showed a consistent upward trajectory with increasing Reynolds number, reaching critical values at Reynolds 200 for specific configurations. The study also highlighted the influence of turbulence, friction, and flow velocity on these results, particularly emphasizing the impact of boundary layer effects and wall proximity. The presence of a moving wall within the investigated gap was found to play a role in maintaining laminar flow and reducing vortex shedding disturbances. It was noted that the scenario of a cylindrical object positioned between two fixed walls resulted in the highest flow fluctuations and

Nusselt number variations. As a result, the comprehensive comparison of Nusselt and Strouhal numbers, lift and drag coefficients in this study with the referenced articles highlights the significance of understanding the intricate dynamics of fluid flow around obstacles. The findings underscore the importance of considering various factors such as Reynolds number, wall proximity, and flow disturbances in optimizing heat transfer processes and energy efficiency in practical applications. The analysis of drag coefficients across different configurations provides valuable insights into the complex interplay between flow characteristics and geometric parameters. Moving forward, further research focusing on refining numerical models and experimental validations can contribute to advancing our knowledge of fluid dynamics and enhancing the design of efficient thermal management systems.

Nomenclature

D	Cylinder diameter [m]
St	Strouhal number
U	Freestream velocity [m/s]
Nu	Time and surface-averaged Nusselt number
u	Streamwise velocity in the x direction [m/s]
T	Temperature [K]
v	Cross-stream velocity in the y direction [m/s]
ρ	Fluid Viscosity [kg/m^3]
P	Flow pressure
G	Gap size [m]
V	The speed of the walls [m/s]
Cd_{ave}	Time-mean drag coefficient
Re	Reynolds number
Cl_{rms}	Root mean square-lift coefficient
NMW-1	Circular cylinder near to a stationary wall (gap = 2D)
NMW-2	Circular cylinder near to two stationary walls (gap = 2D)
NSW-1	Circular cylinder near to a moving wall (gap = 2D)
FSW	Circular cylinder far from stationary Walls (unbounded cylinder)
NS&MW	Circular cylinder near to two walls (one stationary and one moving) (gap = 2D)
NSW-2	Circular cylinder near to two stationary walls (gap = 2D)

References

- [1] Kiyumarsioskouei, A., & Taraghi Osguei, A. (2023). Time and frequency analysis of fluctuating hydrodynamic forces acting on circular and square cylinders in laminar flows. *Journal of the Brazilian Society of Mechanical Sciences and Engineering*, 45(6), 295.

- [2] Wu, M. H., Wen, C. Y., Yen, R. H., Weng, M. C., & Wang, A. B. (2004). Experimental and numerical study of the separation angle for flow around a circular cylinder at low Reynolds number. *Journal of Fluid Mechanics*, 515, 233-260.
- [3] Braza, M., Chassaing, P. H. H. M., & Minh, H. H. (1986). Numerical study and physical analysis of the pressure and velocity fields in the near wake of a circular cylinder. *Journal of fluid mechanics*, 165, 79-130.
- [4] Ahmad, R. A. (1996). Steady-state numerical solution of the Navier-Stokes and energy equations around a horizontal cylinder at moderate Reynolds numbers from 100 to 500. *Heat Transfer Engineering*, 17(1), 31-81.
- [5] Zhou, S., Zhang, G., & Xu, X. (2022). Experiments on the Drag and Lift Coefficients of a Spinning Sphere. *Water*, 14(17), 2593.
- [6] Ghasemian, M., & Nejat, A. (2015). Aerodynamic Noise computation of the flow field around NACA 0012 airfoil using large eddy simulation and acoustic analogy. *Journal of Computational Applied Mechanics*, 46(1), 41-50.
- [7] Lei, C., Cheng, L., Armfield, S. W., & Kavanagh, K. (2000). Vortex shedding suppression for flow over a circular cylinder near a plane boundary. *Ocean Engineering*, 27(10), 1109-1127.
- [8] Zdravkovich, M. M. (1981). Review and classification of various aerodynamic and hydrodynamic means for suppressing vortex shedding. *Journal of Wind Engineering and Industrial Aerodynamics*, 7(2), 145-189.
- [9] Cai, J. C., Pan, J., Kryzhanovskiy, A., & E, S. J. (2018). A numerical study of transient flow around a cylinder and aerodynamic sound radiation. *Thermophysics and Aeromechanics*, 25(3), 331-346.
- [10] Bouakkaz, R., Talbi, K., Khelil, Y., Salhi, F., Belghar, N., & Ouazizi, M. (2014). Numerical investigation of incompressible fluid flow and heat transfer around a rotating circular cylinder. *Thermophysics and Aeromechanics*, 21, 87-97.
- [11] Hussain, L., & Khan, M. M. (2021). Passive Control of Vortex Shedding and Drag Reduction in Laminar Flow across Circular Cylinder Using Wavy Wall Channel. *Fluid Dynamics*, 56, 262-277.
- [12] Taneda, S. (1965). Experimental investigation of vortex streets. *Journal of the Physical Society of Japan*, 20(9), 1714-1721.
- [13] Yoon, H. S., Lee, J. B., & Chun, H. H. (2007). A numerical study on the fluid flow and heat transfer around a circular cylinder near a moving wall. *International Journal of Heat and Mass Transfer*, 50(17-18), 3507-3520.
- [14] de Oliveira, M. A., & Alcântara Pereira, L. A. (2022). A Lagrangian roughness model integrated with the vortex method for drag coefficient estimation and flow control investigations around circular cylinder for a wide range of Reynolds numbers. *Journal of the Brazilian Society of Mechanical Sciences and Engineering*, 44(8), 331.
- [15] Dai, S., Younis, B. A., Zhang, H., & Guo, C. (2018). Prediction of vortex shedding suppression from circular cylinders at high Reynolds number using base splitter plates. *Journal of Wind Engineering and Industrial Aerodynamics*, 182, 115-127.
- [16] Ghoreishi, S. M. N., & Mehri Khansari, N. (2023). Mode (I, II, III) Stress Intensity Factors of Composite-Coated Gas Turbine Blade Using Semi-Elliptical Crack. *Iranian Journal of Science and Technology, Transactions of Mechanical Engineering*, 47(4), 1841-1857.
- [17] Ghoreishi, S. M. N., Mehri-Khansari, N., & Rezaei, H. (2022). Mixed Mode (I/II/III) Stress Intensity Factors in Gas Turbine Blade Considering 3D Semi-elliptical Crack. *Journal of Aerospace Science and Technology*, 15(1), 1-13.
- [18] Chen, L., Dong, Y., & Wang, Y. (2021). Flow-induced vibration of a near-wall circular cylinder with a small gap ratio at low Reynolds numbers. *Journal of Fluids and Structures*, 103, 103247.
- [19] Yoon, H. S., Chun, H. H., Ha, M. Y., & Lee, H. G. (2004). A numerical study on the fluid flow and heat transfer around a circular cylinder in an aligned magnetic field. *International Journal of Heat and Mass Transfer*, 47(19-20), 4075-4087.
- [20] KS, A. (2020). Heat transfer in magnetohydrodynamic nanofluid flow past a circular cylinder. *Physics of Fluids*, 32(4).
- [21] Price, S. J., Sumner, D., Smith, J. G., Leong, K., & Paidoussis, M. P. (2002). Flow visualization around a circular cylinder near to a plane wall. *Journal of Fluids and Structures*, 16(2), 175-191.
- [22] Liu, Y., Liu, J., & Gao, F. P. (2023). Strouhal number for boundary shear flow past a circular cylinder in the subcritical flow regime. *Ocean Engineering*, 269, 113574.

- [23] Faraji Oskouie, M., & Ansari, R. (2021). Vibration analysis of fractional viscoelastic CNTs conveying fluid resting on fractional viscoelastic foundation considering nonlocal effects. *Computational Sciences and Engineering*, 1(2), 123-137.
- [24] Molochnikov, V. M., Mikheev, N. I., Mikheev, A. N., & Paereliy, A. A. (2017). Heat transfer from a cylinder in pulsating cross-flow. *Thermophysics and Aeromechanics*, 24(4), 569-575.
- [25] Park, J., Kwon, K., & Choi, H. (1998). Numerical solutions of flow past a circular cylinder at Reynolds numbers up to 160. *KSME international Journal*, 12, 1200-1205.
- [26] Isaev, S. A., Baranov, P. A., Zhukova, Y. V., & Sudakov, A. G. (2014). Enhancement of heat transfer in unsteady laminar oil flow past a heated cylinder at $Re=150$. *Thermophysics and Aeromechanics*, 21(5), 531-544.
- [27] Sanitjai, S., & Goldstein, R. J. (2004). Forced convection heat transfer from a circular cylinder in crossflow to air and liquids. *International journal of heat and mass transfer*, 47(22), 4795-4805.
- [28] Kumar, D., Layek, A., & Kumar, A. (2023). Enhancement of thermal efficiency and development of Nusselt number correlation for the solar air heater collector roughened with artificial ribs for thermal applications. *Environmental Science and Pollution Research*, 1-15.
- [29] Kohansal Vajargah, M., & Zanganeh Mahalleh, K. (2022). Energy, Exergy and Economic Analysis of a Multi-Generation System Using the Waste Heat of a Wind Turbine. *Computational Sciences and Engineering*, 2(2), 251-274.
- [30] Sobamowo, G., Ajayi, A. B., Oyekeye, M. O., & Adeleye, O. A. (2022). Thermal-Fluidic Study of Drying Chamber of Photovoltaic-powered Forced Convection Solar Dryer using Finite Element Method. *Computational Sciences and Engineering*, 2(2), 181-199.
- [31] Senthilkumar, R., Prabhu, S., & Premalatha, V. (2023). Numerical investigation and optimization of laminar cross flow confinement effects and information fusion on heated circular cylinder using TOPSIS method. *Journal of the Brazilian Society of Mechanical Sciences and Engineering*, 45(4), 214.
- [32] Lei, C., Cheng, L., & Kavanagh, K. (1999). Re-examination of the effect of a plane boundary on force and vortex shedding of a circular cylinder. *Journal of Wind Engineering and Industrial Aerodynamics*, 80(3), 263-286.
- [33] Ding, H., Shu, C., Yeo, K. S., & Xu, D. (2007). Numerical simulation of flows around two circular cylinders by mesh-free least square-based finite difference methods. *International journal for numerical methods in fluids*, 53(2), 305-332.
- [34] Alam, M. M., Moriya, M., Takai, K., & Sakamoto, H. (2003). Fluctuating fluid forces acting on two circular cylinders in a tandem arrangement at a subcritical Reynolds number. *Journal of Wind Engineering and Industrial Aerodynamics*, 91(1-2), 139-154.
- [35] Mahir, N., & Altaç, Z. (2008). Numerical investigation of convective heat transfer in unsteady flow past two cylinders in tandem arrangements. *International Journal of Heat and Fluid Flow*, 29(5), 1309-1318.